Published in final edited form as:
Circulation. 2004 April 27; 109(16): 2023–2029. doi:10.1161/01.CIR.0000127034.50006.C0.

In Vivo Molecular Imaging of Acute and Subacute Thrombosis Using a Fibrin-Binding Magnetic Resonance Imaging Contrast Agent

René M. Botnar, PhD, **Alexandra S. Perez, BS**, **Sonia Witte, PhD**, **Andrea J. Wiethoff, PhD**, **James Laredo, MD, PhD**, **James Hamilton, PhD**, **William Quist, MD**[†], **Edward C. Parsons Jr, PhD**, **Anand Vaidya, BS**, **Andrew Kolodziej, PhD**, **John A. Barrett, PhD**, **Philip B. Graham, PhD**, **Robert M. Weisskoff, PhD**, **Warren J. Manning, MD**, and **Michael T. Johnstone, MD**
Departments of Medicine, Cardiovascular Division (R.M.B., A.S.P., A.V., W.J.M., M.T.J.), Radiology (W.J.M.), Surgery (J.L.), and Pathology (W.Q.), Beth Israel Deaconess Medical Center and Harvard Medical School, Boston, Mass; Boston University School of Medicine, Boston, Mass (J.H.); and EPIX Medical Inc, Cambridge, Mass (S.W., A.J.W., E.C.P., A.K., J.A.B., P.B.G., R.M.W.)

Abstract

Background—Plaque rupture with subsequent thrombosis is recognized as the underlying pathophysiology of most acute coronary syndromes and stroke. Thus, direct thrombus visualization may be beneficial for both diagnosis and guidance of therapy. We sought to test the feasibility of direct imaging of acute and subacute thrombosis using MRI together with a novel fibrin-binding gadolinium-labeled peptide, EP-1873, in an experimental animal model of plaque rupture and thrombosis.

Methods and Results—Fifteen male New Zealand White rabbits (weight, ≈3.5 kg) were made atherosclerotic by feeding a high-cholesterol diet after endothelial aortic injury. Plaque rupture was then induced with the use of Russell's viper venom (RVV) and histamine. Subsequently, MRI of the subrenal aorta was performed before RVV, after RVV, and after EP-1873. Histology was performed on regions suggested by MRI to contain thrombus. Nine rabbits (60%) developed plaque rupture and thrombus, including 25 thrombi visually apparent on MRI as "hot spots" after injection of EP-1873. Histological correlation confirmed all 25 thrombi (100%), with no thrombi seen in the other regions of the aorta. In the remaining 6 rabbits (control) without plaque rupture, no thrombus was observed on the MR images or on histology.

Conclusions—We demonstrate the feasibility of in vivo "molecular" MRI for the detection of acute and subacute thrombosis using a novel fibrin-binding MRI contrast agent in an animal model of atherosclerosis and acute/subacute thrombosis. Potential clinical applications include thrombus detection in acute coronary syndromes and stroke.

Keywords

imaging; fibrin; thrombosis; contrast media; magnetic resonance imaging

Correspondence to René M. Botnar, PhD, Beth Israel Deaconess Medical Center, Cardiovascular Division, Cardiac MR Center, 330 Brookline Ave, Boston, MA 02215. rbotnar@bidmc.harvard.edu.
[†]Deceased.
Reprint requests to Michael T. Johnstone, MD, Cardiovascular Division, 330 Brookline Ave, Boston, MA 02215. mjohnst1@bidmc.harvard.edu

Despite advances in both treatment and prevention, atherosclerotic disease remains the leading cause of morbidity and mortality in the Western world. Although atherosclerosis may progress slowly over many years, thrombosis as a consequence of sudden plaque rupture may lead to abrupt life-threatening complications, including acute coronary syndromes and stroke.[1,2] For those presenting with symptoms for <6 hours, thrombolytic therapy is often advocated.[3] Thus, direct thrombus visualization in such patients may be beneficial for both diagnosis and therapy.

Although a variety of invasive imaging modalities such as intravascular ultrasound elastography,[4] x-ray angiography,[5] angioscopy,[6] and thermography[7] have been used for imaging vulnerable plaques, MRI has emerged as the most promising noninvasive imaging technique for the in vivo detection and characterization of atherosclerotic lesions.[8–10] Recent studies also have shown high sensitivity of MRI to the detection of carotid and aortic thrombi.[11–13] However, differentiation between complex atherosclerotic plaques and mural thrombosis remains difficult because of the complex composition (eg, platelets, fibrin, and red blood cells[13]) of thrombus and resultant complex MR signal characteristics on T1-, T2-, and proton density–weighted images of arterial thrombi.

Recent advances in the field of molecular imaging have led to the development of novel paramagnetic and superparamagnetic targeted MR contrast agents that bind exclusively to molecules such as albumin, fibrin, or angiogenesis markers.[14,15] Because of the inherently low sensitivity of MR contrast enhancement technology, a relatively high target molecule concentration is necessary for adequate signal amplification. Fibrin is abundant in arterial thrombi. We therefore tested a novel fibrin-binding, clot-enhancing contrast agent composed of a gadolinium-labeled peptide derivative (4 Gd molecules per peptide), EP-1873 (EPIX Medical Inc), for its potential to enhance contrast between thrombus, blood, and the underlying plaque. Here we report results for in vivo imaging in a rabbit model of plaque rupture and acute thrombosis.

Methods

Synthesis and fibrin specificity data of EP-1873 are presented in the Appendix.

Animal Model of Plaque Rupture and Thrombosis

Balloon injury of the abdominal aortic wall was performed in 15 adult male New Zealand White rabbits (weight, ≈3.5 kg; Millbrook Immunoserv, Amherst, Mass) with a 3F Fogarty catheter (model EMB40) introduced through a right femoral artery cutdown. Animals were induced with ketamine (35 mg/kg IM), xylazine (2.5 mg/kg IM), and acepromazine (0.75 mg/kg IM) and anesthetized with isoflurane inhalation via mask. After the surgical procedure, rabbits were housed and fed a high-cholesterol diet (Purina modified 1% cholesterol diet 5736C-G) for an 8-week period.

Pharmacological Trigger

After the 8-week high-cholesterol diet, plaque rupture was induced with the use of Russell's viper venom (RVV) (0.15 mg/kg IP; Sigma Chemical Co) and histamine (0.02 mg/kg IV) (Figure 1).[11] Rabbits that did not develop histological apparent plaque rupture with subsequent thrombosis served as a negative control group. Immediately after the MRI, animals were killed by bolus injection of sodium pentobarbital (100 mg/kg IV). Subsequently, the aorta was excised, cut into 3-mm sections, embedded in tissue-freezing medium (TBS; Fisher Scientific), snap-frozen, and stored at −80° until histopathologic analysis.

MRI Experiments

MRI experiments were performed on 2 groups of animals: acute (n=7) and subacute (n=8) thrombosis. In both groups, MRI of the subrenal aorta was performed before administration of RVV (baseline) and after administration of RVV and histamine and subsequently after injection of EP-1873 (Figure 1). Rabbits were anesthetized with ketamine (35 mg/kg IM) and xylazine (5 mg/kg IM) and scanned in the supine position.

Acute Thrombosis Group

To test the ability of EP-1873 for direct in vivo detection of acute thrombosis after plaque rupture, EP-1873 (2 μmol/kg) was injected intravenously approximately 1 hour (1.1±1.2 hours; range, 0.25 to 3.75 hours; n=7) after the pharmacological trigger (Figure 1). Early imaging was performed approximately 30 minutes after EP-1873. After the early imaging session, rabbits were returned to the animal facility for recovery. Twenty-four hours later, rabbits were again anesthetized, and delayed MRI was performed. All studies were performed under the approval of the hospital Animal Care and Use Committee on Animal Investigations.

Subacute Thrombosis Group

Because many patients suffering from acute coronary syndromes or stroke present “late” with subacute (>1 to 3 days) thrombosis, we additionally sought to determine whether EP-1873 can enhance a subacute thrombus. Similar to the experiment of acute thrombosis, pharmacological triggering was used to induce plaque rupture; however, EP-1873 contrast injection was delayed for 1 to 3 days (49±20 hours; n=8) after pharmacological trigger to allow thrombus formation (1 to 3 days) before administration of EP-1873 (Figure 1). Similar to the experiment of acute thrombosis, we performed early and delayed imaging after EP-1873 injection.

MRI Sequence

All scans were performed on a 1.5-T Philips Gyroscan ACS-NT scanner (Philips Medical Systems) with the use of a 5-element cardiac synergy coil for signal reception and an advanced cardiac software package (R8.1.3). After localization of the subrenal aorta with a rapid multislice (10 slices per stack), multistack (transverse, coronal, sagittal), fast gradient-echo scout scan, high-resolution cross-sectional images of the aortic vessel wall were acquired with the use of a nontriggered, fat-suppressed, 3D, T1-weighted gradient-echo sequence covering the entire subrenal aorta (2 stacks). Imaging parameters include repetition time=43 ms, echo time=4.3 ms, flip angle=30°, field of view=60 mm, matrix=196×196, slice thickness=3 mm, spatial resolution=0.3×0.3×3 mm, reconstructed resolution=0.1×0.1×1.5 mm, slices=20, and averages=2. Superior and inferior saturation bands (80 mm thick) were applied for blood signal suppression. Total imaging time per 3D stack was approximately 7 minutes. Scanning was typically performed for 2 hours after injection of EP-1873.

Signal-to-Noise Ratio and Contrast-to-Noise Ratio Measurements

Signal-to-noise ratio (SNR) of thrombus was determined by manually segmenting the visually apparent thrombus area and calculating the mean signal (S). Noise (N) was determined within a region of interest drawn outside of the animal. Contrast-to-noise ratio [$CNR=(S_{thrombus}-S_{blood/muscle})/N$] was measured between thrombus and aortic blood (S_{blood}) and thrombus and adjacent muscle (S_{muscle}), respectively.

Histology

Thrombus detection was performed by gross histological analysis of the entire subrenal aorta and by subsequent sectioning and immuno-histological analysis. All sections (slice thickness=5 μm, every 3 mm, cryostat sectioned) starting at the right renal artery and continuing inferiorly to the aortic bifurcation were stained with hematoxylin and eosin and assessed visually (unblinded; A.S.P.) for the presence or absence of thrombus. Histological cross sections (every 3 mm) were then compared with the corresponding MRI slices with the aortic bifurcation used as common reference point.

Statistical Analysis

Data are expressed as mean±1 SD. Continuous variables were compared with a 2-tailed, paired, Student *t* test, with significance set at $P \leq 0.05$.

Results

MRI Before Plaque Rupture

No evidence of thrombus was present on native MR images before pharmacologically induced plaque rupture in any of the animals.

Fibrin-Targeted MRI

When the acute and subacute groups were combined, plaque rupture with overlying thrombus was observed in 9 (60%) of 15 rabbits after administration of RVV and histamine. In these 9 animals, 25 thrombi were detected as visually apparent “hot spots” by MRI after injection of EP-1873, with high contrast between thrombus, thrombus-free vessel wall, and blood (Figures 2 and 3). Histological correlation confirmed all 25 thrombi (100%), with no histological evidence for thrombus in the other regions of the aorta. Average thrombus length on MRI was 14±11 mm (range, 3 to 51 mm). The remaining 6 (40%) of 15 rabbits did not show histological evidence for thrombus or MR evidence (“hot spot”) of thrombus.

Because of the high MRI signal intensity of EP-1873–enhanced thrombi, targeted maximum intensity projections (MIPs) of the aorta could be created and allowed ready depiction of focal thrombi in the subrenal aorta (Figure 4). On the precontrast MIPs, detection of plaque versus thrombus was difficult because of the low contrast between thrombus, wall, and lumen.

Additional higher-resolution (0.4×0.4×1.3 mm) 3D scans (Figure 5) along the course of the aorta allowed clear depiction of mural thrombi with respect to landmarks such as the renal arteries or the aortic bifurcation.

Imaging of Acute Thrombus

Five (71%) of 7 rabbits undergoing MRI developed plaque rupture with subsequent thrombosis. Early and delayed imaging findings are discussed below.

Early and Delayed Imaging—After injection of EP-1873, early imaging was initiated at approximately 10 minutes (0.2±0.1 hours) and was repeated until approximately 2 hours. Administration of RVV and histamine led to visible vasoconstriction of the subrenal aorta compared with the baseline images (Figure 2A and 2B), with no visual evidence of thrombosis on the 30 minutes post-RVV scan (Figure 2B). Immediately after injection of EP-1873, focal signal enhancement (arrow) was readily apparent on the postcontrast T1-weighted images (Figure 2C), suggestive of ruptured plaque with mural thrombus. The focal area increased in size and signal intensity over the subsequent 6 hours despite no further

administration of EP-1873 (Figure 2D and 2E), suggesting ongoing thrombus formation. Thirty minutes after contrast injection, modest venous and arterial blood pool signal enhancement was observed (Figure 2C). This enhancement subsequently declined, leading to a steady increase in CNR between thrombus and arterial blood. Persistence of thrombus signal intensity was investigated with the use of delayed imaging, with the latest images acquired 23±12 hours after EP-1873 injection. Good thrombus delineation was observed in the later acquired images (Figure 2E), with good contrast between thrombus and blood. Corresponding histology section shows a thrombus overlying a thickened vessel wall (Figure 2F).

Average CNR between thrombus and blood was 12±7 (1 hour after EP-1873) and rose to 24±10 (20 hours after EP-1873; $P<0.001$). Slightly lower CNR values were found between thrombus and muscle (1 hour after EP-1873: 7±7; 20 hours after injection: 16±8; $P<0.001$). Average thrombus SNR rose from 18±8 (1 hour after EP-1873) to 28±10 (20 hours after EP-1873; $P<0.01$). Average arterial blood SNR increased from 4.5±1.2 (baseline) to 5.8±2.0 (1 hour after EP-1873; $P<0.05$) and returned to 4.2±1.2 (20 hours after EP-1873; P=NS versus baseline).

Imaging of Subacute Thrombus

Four (50%) of 8 rabbits developed plaque rupture with subsequent thrombosis. Early and delayed imaging findings in the subacute animals are discussed below.

Early and Delayed Imaging—On the baseline pretrigger images (Figure 3A), no visually apparent thrombus was observed. Twenty-four hours after administration of RVV and histamine (Figure 3B), a lumen-encroaching mass/thrombus could be seen, consistent with interim thrombus development. Thirty minutes after administration of EP-1873, signal enhancement along the surface of the thrombus was observed (Figure 3C). This signal enhancement increased at 60 minutes (Figure 3D). Delayed imaging at 20 hours after the administration of EP-1873 (Figure 3E) showed strong signal enhancement of both deep and superficial portions of the thrombus, with good delineation from arterial blood and thrombus-free vessel wall. Good agreement in shape and location was found with histopathology (Figure 3F).

CNR between native thrombus and blood was 8±2 and rose to 10±3 at 1 hour after injection of EP-1873 ($P<0.01$) and further increased to 19±7 (20 hours after EP-1873; $P<0.001$ versus native). Similar to the acute thrombus experiment, lower CNR values were found between thrombus and muscle (native thrombus: 2±1; 1 hour after EP-1873: 5±2; $P<0.001$; 20 hours after EP-1873: 11±6; $P<0.001$). Average thrombus SNR rose from 10±4 (native thrombus) to 15±3 (1 hour after EP-1873; $P<0.01$) and subsequently to 23±7 (20 hours after EP-1873; $P<0.001$).

There was no significant difference in thrombus SNR/CNR (after EP-1873) between the acute and subacute group (P=NS; unpaired t test). Furthermore, no significant correlation ($R^2<0.14$) was found between thrombus size and SNR or CNR.

Discussion

In this study, we demonstrated the successful use of a small-molecule fibrin-binding peptide derivative for noninvasive in vivo MRI of acute and subacute thrombosis after plaque rupture in an animal model of atherosclerosis. EP-1873 permitted imaging of large lumen-encroaching thrombi as well as submillimeter mural thrombi with signal enhancement of the entire thrombus and good differentiation from thrombus-free segments of the vessel wall (better than in a previous study without contrast agent[11]). Differentiation between thrombus

and the underlying ruptured vessel wall was limited, likely as a result of spatial resolution issues and/or contrast agent leakage into the ruptured wall. Experiments of subacute thrombosis showed the potential of the small peptide derivative to enhance already existing thrombi, with early signal enhancement at the clot surface followed by signal enhancement of the entire thrombus (several hours after contrast administration). These findings therefore encourage the application of the presented principles to other markers of plaque vulnerability such as vascular adhesion molecule-1 or matrix metalloproteinase.

Related Work

Compared with previous ex vivo and in vivo (in situ) animal studies by Flacke et al[15] and Johansson et al,[16] we imaged acute and subacute thrombi in an in vivo animal atherosclerosis model of plaque rupture and thrombosis after systemic contrast injection. Although the process of plaque rupture in this model might be different from that in humans, the model reproducibly produces in vivo thrombi at a rate of approximately 60%.

The concept of targeted imaging has been tested with other imaging modalities. Nuclear imaging and ultrasound have been used to target atherosclerotic plaques with the use of either radiolabeled antibodies[17,18] or echogenic liposomes,[19] respectively. However, these techniques had relatively low spatial resolution. Recently, fluorescence imaging with the use of near infrared optical methods has been applied with great success for imaging of gene expression[20,21] or matrix metalloproteinase inhibition[22] in genetically engineered mice. This approach suffers from a limited penetration depth, and it remains to be proven whether optical methods will play a role in a clinical setting.

In recent studies by Flacke et al[15] and Yu et al,[14] ex vivo and in vivo (in situ) MRI detection of human plasma clots and canine thrombus were demonstrated with the use of gadolinium-loaded lipid-encapsulated perfluorocarbon nanoparticles. The payload of 1 nanoparticle varied between 10 000 and 50 000 gadolinium molecules. Another study by Johansson and colleagues[16] used an ultrasmall superparamagnetic iron oxide coupled to a cyclic arginine-glycine–aspartic acid peptide. Contrast enhancement with the second approach was limited to the clot surface. In the present study, we demonstrated that the small-molecule peptide derivative was able to enhance new thrombus (aged <48 hours) and that 4 gadolinium molecules per peptide appear sufficient to create an MRI signal for visualization of very small microthrombi. Furthermore, we demonstrated that even with a relatively low dose (2 μmol EP-1873 per kilogram), all thrombi were readily detected.

Early and Delayed Imaging

We further demonstrated that the small-molecule fibrin-binding agent enhances subacute thrombi, thus not limiting signal enhancement to the thrombus surface but enabling signal enhancement of the entire thrombus. Continued penetration of thrombus with EP-1873, as seen in all the experiments, may be due to reorganizing processes (platelet rich→fibrin rich) and diffusion. Preliminary simulations support the theory of diffusion-related redistribution of EP-1873 within the thrombus, as observed in Figures 4 and 5. Furthermore, we found evidence that signal enhancement in all thrombi was observed for several hours after contrast injection.

Potential Clinical Applications

Patients with acute coronary syndromes may present with chest pain/symptoms in the absence of diagnostic ECG changes in the emergency department. Early detection of fibrin-rich thrombus may be beneficial for both diagnosis and early treatment.

Noninvasive monitoring of thrombolysis in patients with lumen-encroaching thrombi may be another clinical application that could benefit from this novel approach.

Conclusions

We demonstrate the feasibility of in vivo “molecular” MRI for the detection of acute and subacute thrombosis using a novel fibrin-binding MRI contrast agent in an animal model of atherosclerosis and acute thrombosis. Potential clinical applications include thrombus detection in patients with acute coronary syndromes and stroke.

Acknowledgments

This research was supported in part by a grant from the National Institutes of Health (RO1 HL-61825) (Drs Hamilton and Johnstone) and by EPIX Medical Inc (Cambridge, Mass).

Drs Parsons and Weisskoff are employees of EPIX Medical, which funded the study and furnished the contrast agent.

References

1. Fuster V, Badimon L, Badimon JJ, et al. The pathogenesis of coronary artery disease and the acute coronary syndromes. N Engl J Med 1992;326:242–250. [PubMed: 1727977]
2. Davies MJ, Thomas AC. Plaque fissuring: the cause of acute myocardial infarction, sudden ischaemic death, and crescendo angina. Br Heart J 1985;53:363–373. [PubMed: 3885978]
3. Grotta JC. Adding to the effectiveness of intravenous tissue plasminogen activator for treating acute stroke. Circulation 2003;107:2769–2770. [PubMed: 12796412]
4. de Korte CL, Sierevogel MJ, Mastik F, et al. Identification of atherosclerotic plaque components with intravascular ultrasound elastography in vivo: a Yucatan pig study. Circulation 2002;105:1627–1630. [PubMed: 11940537]
5. Abela GS, Eisenberg JD, Mittleman MA, et al. Detecting and differentiating white from red coronary thrombus by angiography in angina pectoris and in acute myocardial infarction. Am J Cardiol 1999;83:94–97. A8. [PubMed: 10073790]
6. Feld S, Ganim M, Carell ES, et al. Comparison of angioscopy, intravascular ultrasound imaging and quantitative coronary angiography in predicting clinical outcome after coronary intervention in high risk patients. J Am Coll Cardiol 1996;28:97–105. [PubMed: 8752800]
7. Casscells W, Hathorn B, David M, et al. Thermal detection of cellular infiltrates in living atherosclerotic plaques: possible implications for plaque rupture and thrombosis. Lancet 1996;347:1447–1451. [PubMed: 8676628]
8. Toussaint JF, LaMuraglia GM, Southern JF, et al. Magnetic resonance images lipid, fibrous, calcified, hemorrhagic, and thrombotic components of human atherosclerosis in vivo. Circulation 1996;94:932–938. [PubMed: 8790028]
9. Fayad ZA, Fallon JT, Shinnar M, et al. Noninvasive in vivo high-resolution magnetic resonance imaging of atherosclerotic lesions in genetically engineered mice. Circulation 1998;98:1541–1547. [PubMed: 9769308]
10. Yuan C, Mitsumori LM, Ferguson MS, et al. In vivo accuracy of multi-spectral magnetic resonance imaging for identifying lipid-rich necrotic cores and intraplaque hemorrhage in advanced human carotid plaques. Circulation 2001;104:2051–2056. [PubMed: 11673345]
11. Johnstone MT, Botnar RM, Perez AS, et al. In vivo magnetic resonance imaging of experimental thrombosis in a rabbit model. Arterioscler Thromb Vasc Biol 2001;21:1556–1560. [PubMed: 11557688]
12. Corti R, Osende JI, Fayad ZA, et al. In vivo noninvasive detection and age definition of arterial thrombus by MRI. J Am Coll Cardiol 2002;39:1366–1373. [PubMed: 11955857]
13. Moody AR, Murphy RE, Morgan PS, et al. Characterization of complicated carotid plaque with magnetic resonance direct thrombus imaging in patients with cerebral ischemia. Circulation 2003;107:3047–3052. [PubMed: 12796133]

14. Yu X, Song SK, Chen J, et al. High-resolution MRI characterization of human thrombus using a novel fibrin-targeted paramagnetic nanoparticle contrast agent. Magn Reson Med 2000;44:867–872. [PubMed: 11108623]

15. Flacke S, Fischer S, Scott MJ, et al. Novel MRI contrast agent for molecular imaging of fibrin: implications for detecting vulnerable plaques. Circulation 2001;104:1280–1285. [PubMed: 11551880]

16. Johansson LO, Bjornerud A, Ahlstrom HK, et al. A targeted contrast agent for magnetic resonance imaging of thrombus: implications of spatial resolution. J Magn Reson Imaging 2001;13:615–618. [PubMed: 11276107]

17. Mettinger KL, Larsson S, Ericson K, et al. Detection of atherosclerotic plaques in carotid arteries by the use of 123I-fibrinogen. Lancet 1978;1:242–244. [PubMed: 74666]

18. Uehara A, Isaka Y, Hashikawa K, et al. Iodine-131-labeled fibronectin: potential agent for imaging atherosclerotic lesion and thrombus. J Nucl Med 1988;29:1264–1267. [PubMed: 3392585]

19. Demos SM, Onyuksel H, Gilbert J, et al. In vitro targeting of antibody-conjugated echogenic liposomes for site-specific ultrasonic image enhancement. J Pharm Sci 1997;86:167–171. [PubMed: 9040090]

20. Mahmood U, Tung CH, Tang Y, et al. Feasibility of in vivo multichannel optical imaging of gene expression: experimental study in mice. Radiology 2002;224:446–451. [PubMed: 12147841]

21. Wu JC, Inubushi M, Sundaresan G, et al. Optical imaging of cardiac reporter gene expression in living rats. Circulation 2002;105:1631–1634. [PubMed: 11940538]

22. Bremer C, Tung CH, Weissleder R. In vivo molecular target assessment of matrix metalloproteinase inhibition. Nat Med 2001;7:743–748. [PubMed: 11385514]

23. Wiethoff, AJ.; Barrett, JA.; Wang, JF., et al. Pharmacokinetics, biodistribution and efficacy of EP-1873: a Gd-based fibrin specific thrombus MR agent. ISMRM, 11th Annual Meeting; Toronto, Canada. Berkeley, Calif: International Society for Magnetic Resonance in Medicine; 2003. p. 833

24. Etienne A, Botnar RM, Van Muiswinkel AM, et al. “Soap-bubble” visualization and quantitative analysis of 3D coronary magnetic resonance angiograms. Magn Reson Med 2002;48:658–666. [PubMed: 12353283]

Appendix

Synthesis of EP-1873

The cyclic disulfide peptide precursor of EP-1873, [F.H.C.Hyp.Y(3-CI).D.L.C.H.I.L], was prepared with the use of a diaminotryl resin, Fmoc coupling strategy, and thallium trifluoroacetate cyclization. Conjugation of 4 bb-GdDTPA (backbone acid–substituted gadolinium diethylenetriaminepentacetate) moieties was achieved with the use of standard amide coupling chemistry, acid deprotection (trifluoroacetic acid), and subsequent chelation with $GdCl_3$ and NaOH. Purification by reverse-phase high-performance liquid chromatography (C-18 column, ethanol/50 mmol $AcONH_4$) followed by desalting (C-18 SepPak, $EtOH/H_2O$) gave the desired gadolinium complex, EP-1873.

Specificity of EP-1873 and Gd-DTPA for Fibrin

The specificity of EP-1873 for fibrin was tested in a rabbit carotid artery/jugular vein stasis model by coinjection of ^{153}Gd-labeled EP-1873 and ^{111}In-labeled Gd-DTPA (2 μmol/kg each).[23] Chemical analysis showed significantly higher uptake of ^{153}Gd-labeled EP-1873 in carotid thrombus than with ^{111}In-labeled Gd-DTPA (88±36 μmol/L Gd versus 2.5±0.5 μmol/L Gd).[23] Similar results were found for jugular thrombi. Blood levels at 60 minutes after injection were 22±8 and 5.6±1.5 μmol/L Gd for ^{153}Gd-labeled EP-1873 and ^{111}In-labeled Gd-DTPA, respectively. Mean residence time of EP-1873 was 47±10 minutes in plasma. In vitro relaxivity of EP-1873 at 1.4 T and 37°C was 48 and 84 $(\text{mmol/L peptide}\times\text{s})^{-1}$ in buffer and fibrin, respectively.

Binding of EP-1873 to rabbit fibrin was evaluated in Tris-buffered saline, and the K_d was found to be 3.5±0.15 mol/L. The number of binding sites was found to be 2.4±0.1 (Figure 6). Binding to human fibrin was comparable, with a K_d=2.2±0.3 μmol/L and 1.8±0.1 binding sites. In contrast, the K_i for soluble fibrinogen was >200 μmol/L.

Displacement of EP-1873 by Y-1873

To verify that the Gd uptake and consequent T1 shortening effect of EP-1873 is due to the 4 paramagnetic Gd-DTPA molecules bound to its fibrin-specific peptide core, a non-paramagnetic analogue, Y-1873, of EP-1873 was synthesized with Gd replaced by yttrium (Y). Yttrium has negligible MR contrast properties. Displacement of EP-1873 by nonparamagnetic Y-1873 was then demonstrated by MRI in a rabbit carotid artery stasis model. After baseline imaging (Figure 7A), 1.45 μmol/kg EP-1873 was injected, and four 8-minute, T1-weighted, 3D, gradient echo scans (field of view=80 mm, matrix=256×256, repetition time=39 ms, echo time=3.1 ms, slice thickness=0.8 mm, number of slices=64, inferior and superior saturation bands, scan time=8.02 minutes) were acquired to follow signal enhancement of carotid artery thrombus (Figure 7B). A bright ring is evident. At 44 minutes after EP-1873 injection, a 10-fold higher dose (14.5 μmol/kg) of nonparamagnetic Y-1873 was administered. Three additional scans were performed to monitor displacement of EP-1873 (Figure 7C and 7D) by Y-1873. CNR measurements between carotid thrombus and adjacent muscle were done for the entire imaging series. At baseline, thrombus CNR was 0.7 and increased to 9.4 at 30 minutes after EP-1873 injection. Immediately after injection of nonparamagnetic Y-1873, thrombus CNR dropped to 4.4, and by 19 minutes after Y-1873, CNR further decreased to 1.1, demonstrating displacement of fibrin-bound paramagnetic EP-1873 by non-paramagnetic Y-1873.

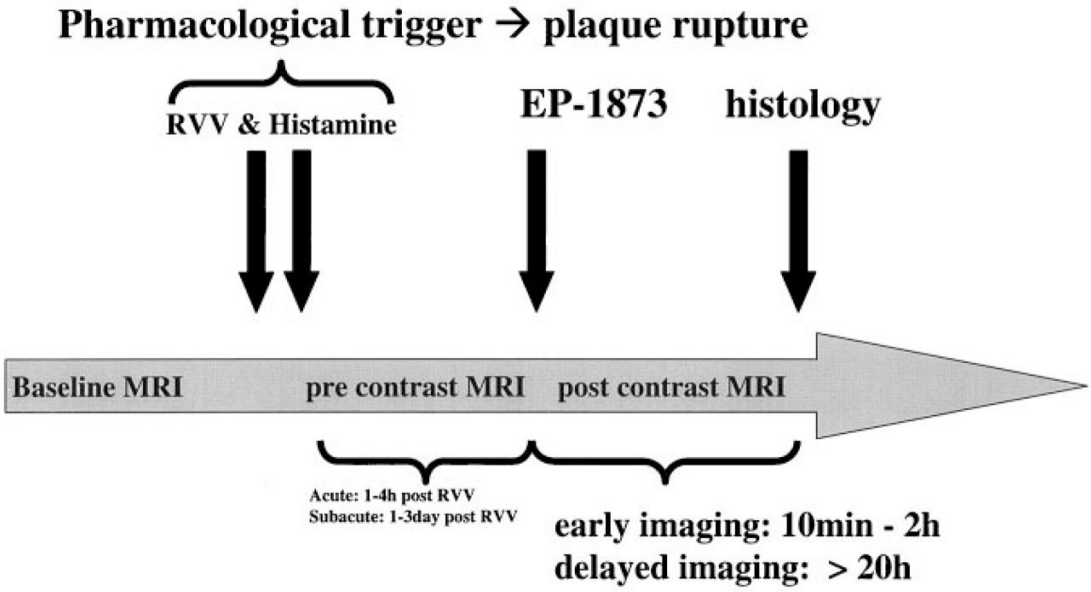

Figure 1.

Time course of in vivo MRI experiment of acute and subacute thrombosis with the use of an atherosclerotic New Zealand White rabbit model. After an 8-week high-cholesterol diet, baseline MRI of the subrenal aorta was performed. Subsequently, plaque rupture was induced with the use of RVV and histamine. The fibrin-binding peptide derivative EP-1873 was then intravenously administered ≈1 hour (imaging of acute thrombosis) or ≈20 hours (imaging of subacute thrombosis) after RVV and histamine. After intravenous injection of EP-1873, MRI was performed at 30 minutes and continued up to ≈20 hours. Subsequently, the animals were killed, and histological analyses were performed.

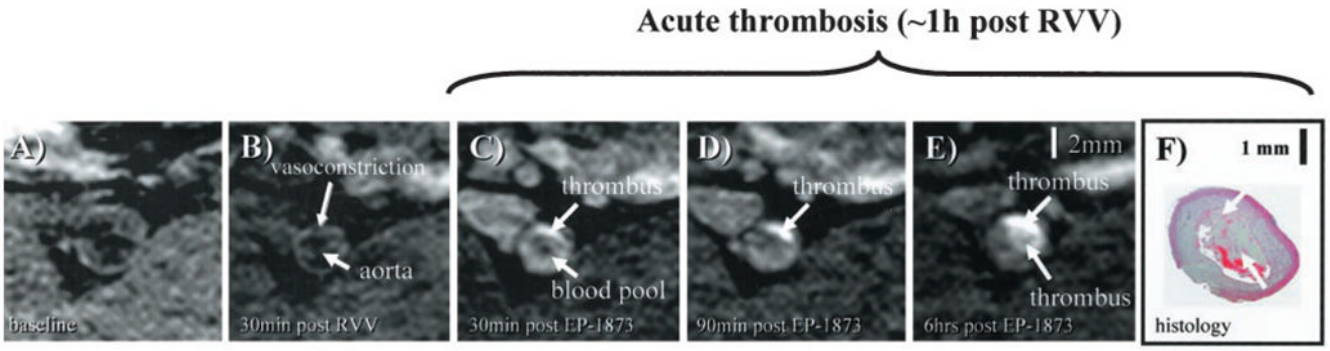

Figure 2.

In vivo visualization of acute thrombosis after plaque rupture induced by RVV and histamine. A, No apparent thrombus is visible on baseline image. B, Thirty minutes after pharmacological triggering with RVV and histamine, vasoconstriction of the subrenal aorta can be observed without obvious signs of thrombosis. C, Thirty minutes after administration of EP-1873, a well-defined bright mass (arrow) can be observed, consistent with a mural thrombus. D, E, Thrombus increased in size and signal intensity over the subsequent 6 hours, consistent with ongoing thrombus formation. F, Histology demonstrates the corresponding thrombus (arrow) overlying a thickened atherosclerotic vessel wall.

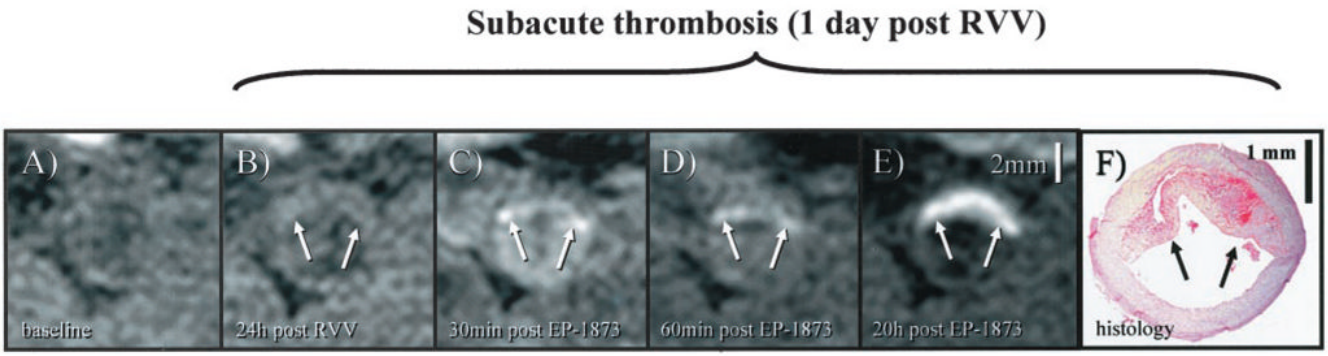

Figure 3.

In vivo visualization of subacute thrombosis after plaque rupture induced by RVV and histamine. A, On the pretrigger baseline image, no apparent thrombosis is visible. B, At 24 hours after trigger, a gray mass (arrow) overlying the vessel wall can be observed, suggestive of a mural thrombus. C, Thirty minutes after EP-1873 injection, a bright rim (arrow) becomes visible along the lumen-facing surface of this mass, which subsequently increased in size and signal intensity, as shown at 60 minutes (D). E, Twenty hours after EP-1873 injection, entire mass (arrow) appeared bright and well defined, suggesting that the fibrin-binding agent had completely penetrated the thrombus. Good agreement was found with thrombus (arrows) on histopathology (F).

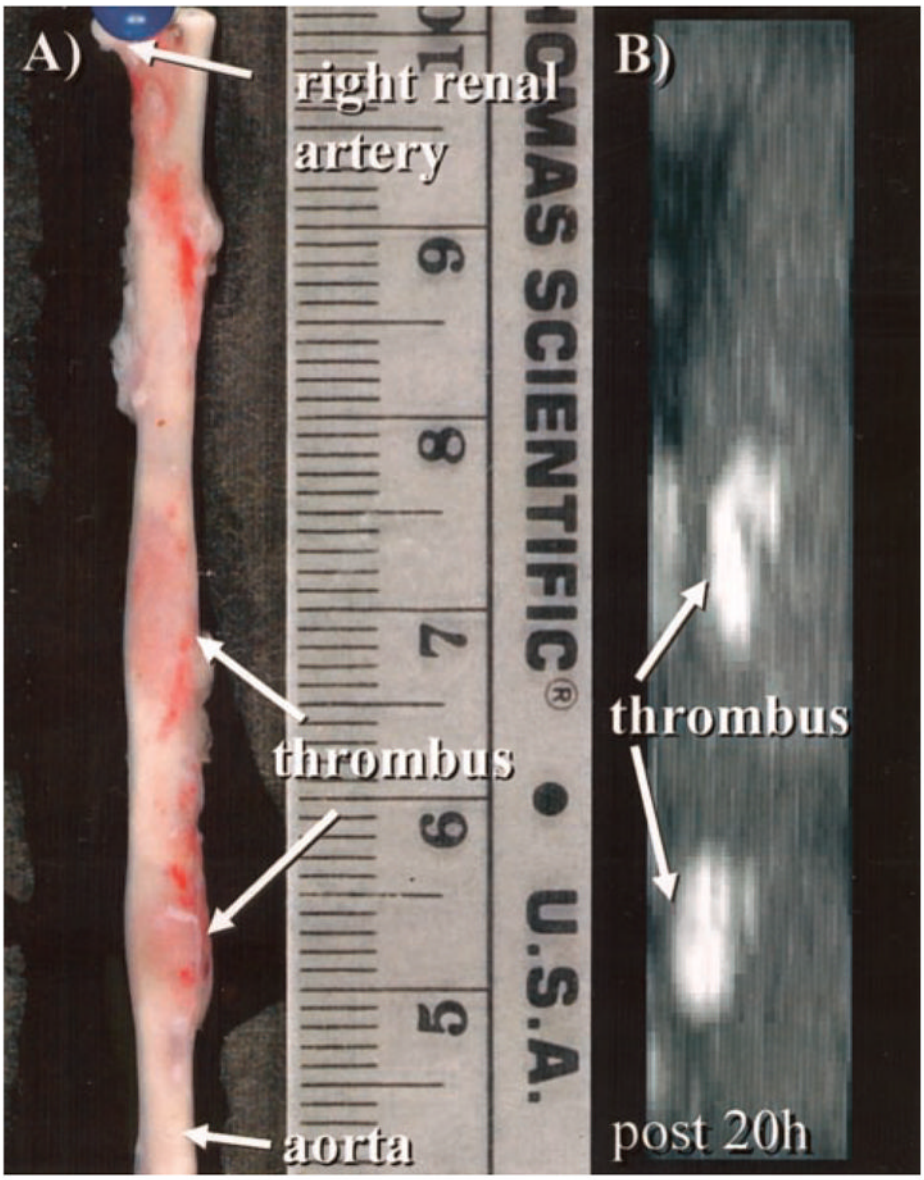

Figure 4.
A, Photograph demonstrates 2 well-delineated focal thrombi (arrows) in a harvested subrenal aorta. B, On corresponding targeted MIP, 2 bright thrombi (arrows) can be identified that correspond in both size and location with gross histological image in A.

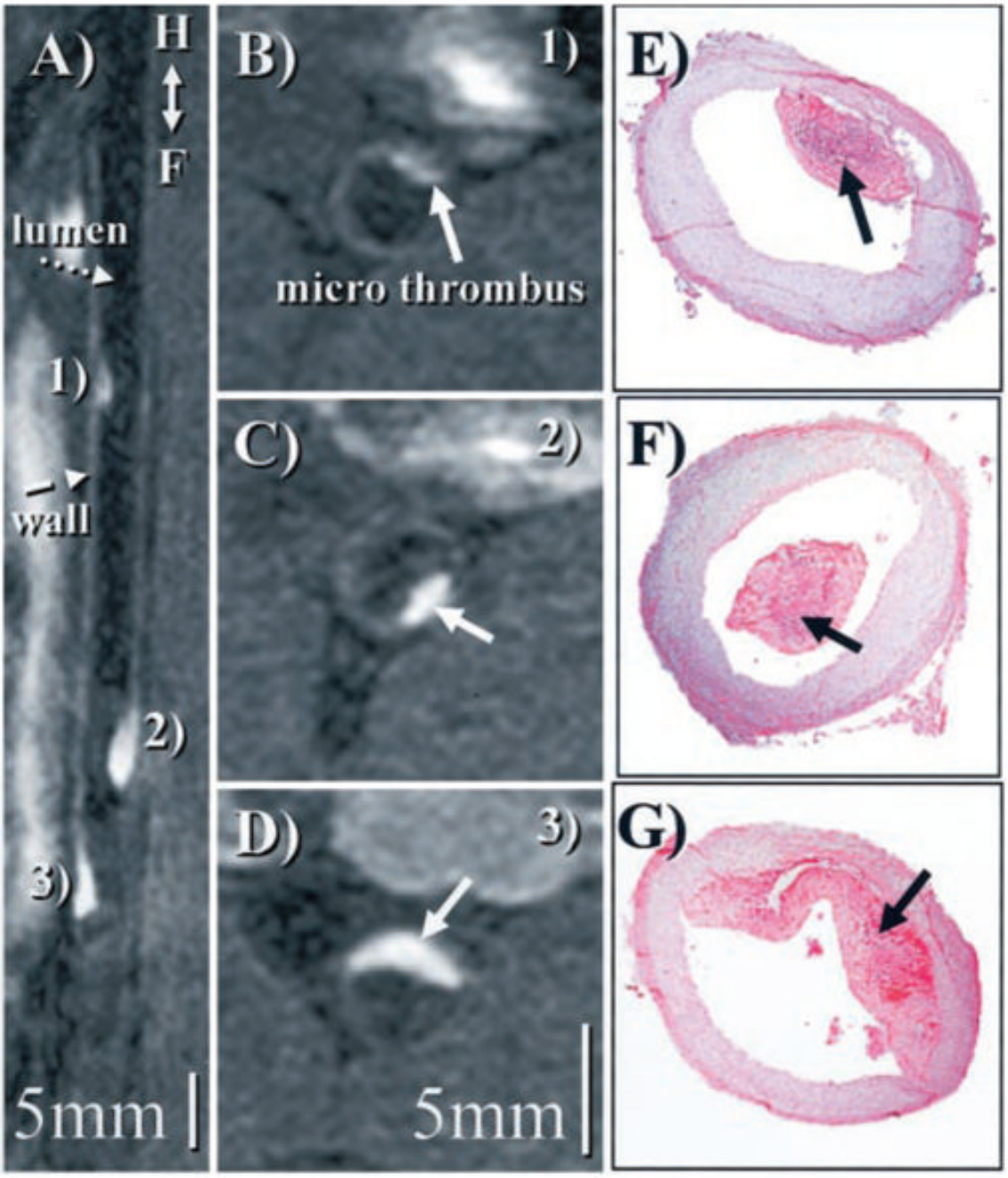

Figure 5.

A, Reformatted view[24] of a coronal 3D data set shows subrenal aorta ≈20 hours after EP-1873 administration. Three well-delineated mural thrombi (arrows) can be observed, with good contrast between thrombus (numbered), arterial blood (dotted arrow), and vessel wall (dashed arrow). The in-plane view of the aorta allows simultaneous display of all thrombi, showing head, tail, length, and relative location. B to D, Corresponding cross-sectional views show good agreement with histopathology (E to G).

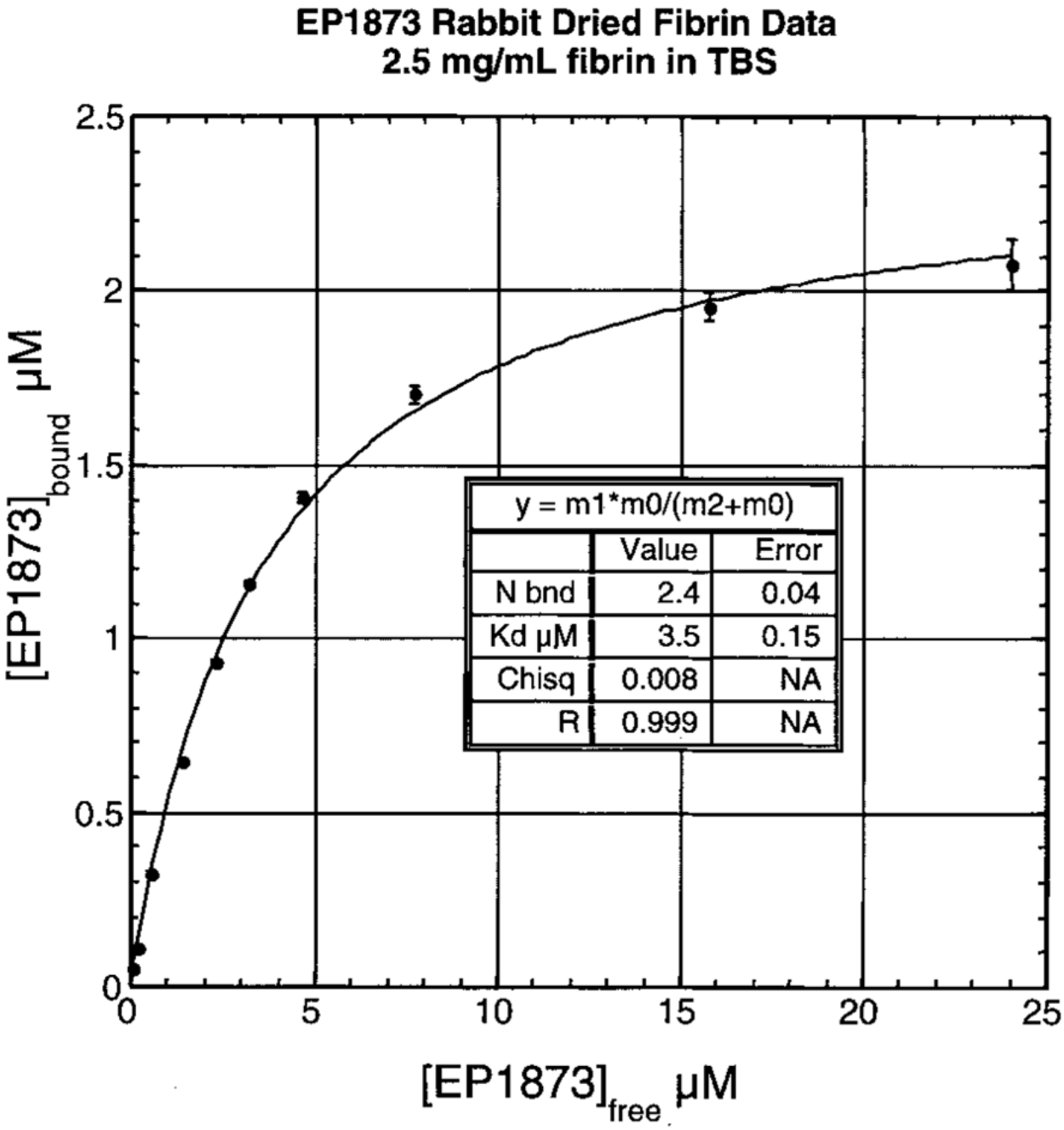

Figure 6.
EP-1873 binding to rabbit fibrin in Tris-buffered saline with data fit best to K_d=3.5±0.15 μmol/L and 2.4±0.1 binding (bnd) sites.

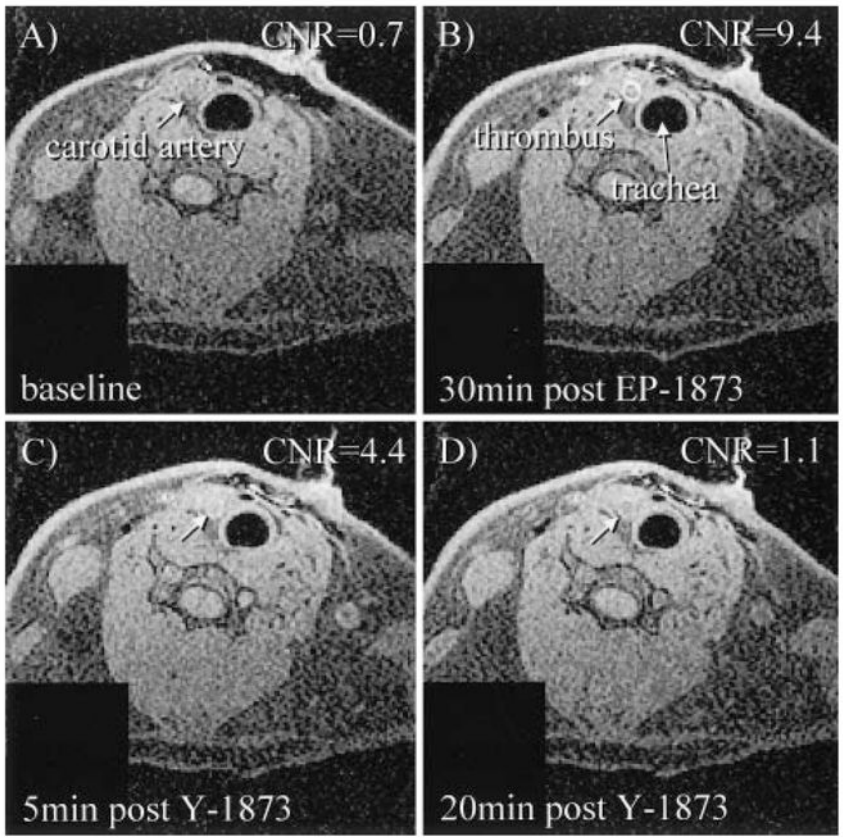

Figure 7.

Displacement of fibrin-bound paramagnetic EP-1873 in a rabbit carotid thrombus model after injection of nonparamagnetic Y-1873. A, Baseline image of carotid artery. B, Carotid thrombus after injection (1.45 μmol/kg) of fibrin-binding EP-1873. C to D, Displacement of paramagnetic EP-1873 by nonparamagnetic Y-1873 (14.5 μmol/kg), resulting in visually apparent decrease of thrombus signal.